Cyclic bond behavior of FRCM composites applied on masonry substrate

Accepted Manuscript

Cyclic bond behavior of Frcm composites applied on masonry substrate

Alessandro Bellini, Seyedmohammad Kahangi Shahreza, Claudio Mazzotti

PII: S1359-8368(19)30636-5

DOI: https://doi.org/10.1016/j.compositesb.2019.04.009

Reference: JCOMB 6748

To appear in: *Composites Part B*

Received Date: 11 February 2019

Revised Date: 28 March 2019

Accepted Date: 6 April 2019

Please cite this article as: Bellini A, Shahreza SK, Mazzotti C, Cyclic bond behavior of Frcm composites applied on masonry substrate, *Composites Part B* (2019), doi: https://doi.org/10.1016/j.compositesb.2019.04.009.

CYCLIC BOND BEHAVIOR OF FRCM COMPOSITES APPLIED ON MASONRY SUBSTRATE

Alessandro Bellini[1,*], Seyedmohammad Kahangi Shahreza[2], Claudio Mazzotti[2]

[1] CIRI Buildings and Construction (CIRI-EC),
University of Bologna, Via del Lazzaretto 15/5, 40131, Bologna, Italy

[2] Department of Civil, Chemical, Environmental and Materials Engineering (DICAM),
University of Bologna, Viale Risorgimento 2, 40136, Bologna, Italy

* Corresponding Author

Tel: +39 051 2090553, email: alessandro.bellini5@unibo.it

ABSTRACT

Fiber Reinforced Cementitious Matrix (FRCM) composite materials represent a recent strengthening technique, which can provide a complex scenario of different mechanical behaviors and failure mechanisms. The presented experimental study is aimed at improving the knowledge about the tensile and bond behavior of FRCMs with a focus, in particular, on the effects of cyclic loading at high stress levels. To this purpose, tensile characterization tests and single-lap shear tests were carried out on six different FRCM types, discussing and clarifying the different bond behaviors and the resulting failure modes. The experimental tests showed that the global behavior of the samples is affected not only by properties of composite grids and mortars, but in particular by the textile-matrix adhesion mechanism. The effects of cyclic loading were experimentally evaluated for each strengthening type in terms of maximum bond capacity, failure mechanism, stress-slip behavior and bond degradation through cycles. In general, application of load cycles didn't remarkably affect the performance of FRCM systems, proving their reliability under seismic forces.

KEYWORDS: FRCM; masonry; bond test; cyclic; degradation.

1. INTRODUCTION

During the last decades, the growing need of extending the service life and improving the seismic capacity of existing masonry buildings encouraged the researchers to study new restoration and strengthening systems.

The advantages of composite-based and hybrid strengthening solutions, such as Fiber Reinforced Polymer (FRP) or Fiber Reinforced Cementitious Matrix (FRCM) materials, are reduced

invasiveness, lightweight, quickness and ease of installation, corrosion resistance, compatibility with other techniques, low-maintenance and effectiveness of the strengthening system [1-7].

However, FRP strengthening systems entail several disadvantages such as very poor permeability, problems at high temperatures, incompatibility of epoxy resins with several substrates, relatively high materials costs and impossibility to make the intervention completely reversible.

In this framework, FRCM composite materials, composed of a fiber textile embedded into an inorganic matrix, represent an innovative class of composites which has been recently introduced to overcome or reduce the disadvantages of epoxy resins.

In fact, replacement of epoxy resins with inorganic matrices leads to several improvements like fire resistance, permeability, applicability on wet surfaces, reversibility, reduction in installation costs and durability [8], key aspects that often made FRCMs preferable to other reinforcement techniques.

The textile used in these composite materials can be constituted of different fibers (e.g. glass, basalt, carbon, steel, PBO, aramid) often present in the form of bi-directional grids, whereas the inorganic matrices are usually cementitious or lime based mortars, sometimes enriched with short fibers.

Despite these technical advantages, there is still a lack of standard codes and recommendations for testing, design and control of these innovative composite materials.

Even if some technical guides are already present in the American framework [9,10], in Europe guidelines and code prescriptions for mechanical characterization of these composite materials, required for the qualification process and for the design, are relatively new [11] or currently in preparation.

Many research works on the tensile characterization and on the bond behavior of FRPs are available nowadays [12-26], but only few studies can be found on the tensile behavior [27] or on the effectiveness of FRCM strengthening systems applied on masonry elements [28-41], with the available experimental database resulting mainly limited to monotonic tests.

In this framework, the present experimental study is aimed at improving the knowledge of mechanical and adhesion properties of FRCMs, by evaluating the tensile behavior and bond performance of these composite materials when applied on masonry substrates, with a focus, in particular, on their cyclic behavior and on the following comparison between monotonic and cyclic tests results.

To this purpose, FRCM specimens made of bi-directional carbon, glass, aramid-glass and basalt grids embedded within natural hydraulic lime (NHL) matrices were prepared for uniaxial tensile tests or applied on masonry substrate for performing single-lap bond tests.

Tensile tests on FRCM specimens, which can provide important parameters such as elastic moduli of the composite during the different phases and its cracking behavior, can be performed according to different set-ups [27, 42-45] and experimental outcomes could be severely influenced by the choice of samples configuration and dimensions, by the production process and by the adopted clamping system.

Between the different shapes [46,47], the rectangular one is the simplest to realize and can be recommended because it can faithfully reproduce the shape of the textile; for this reason, during the experimental campaign here described, a constant rectangular shape has been chosen, without introduce expedients to impose the location of the first crack in a predefined section. This choice allowed to observe the overall behavior of the samples for what concerns failure mechanisms and crack patterns.

The reinforcement geometry adopted for tensile tests has been used also for the realization of the specimens subjected to single-lap shear tests, with the purpose of analyzing and comparing the results without introducing dimension-dependent effects.

As shown by recent experimental studies, FRCM-masonry bond has different peculiarities if compared to FRP-masonry adhesion mechanism.

In fact, whereas bond tests carried out on FRPs showed as a typical failure mode the debonding from the substrate occurring with the detachment of a thin material layer [12,15,17,19,25], FRCM

strengthening systems highlighted much more complicated failure mechanisms, affected by mechanical properties and geometry of grid and mortar [28,32-36,45].

Even if the most common failure modes experienced by several authors [48-51] are the debonding located at the fibers-matrix interface or the slippage of the reinforcement grid within the matrix, the modification or the addition of some components used within the mortar [30] can considerably affect maximum bond capacity and change the predicted failure mechanisms.

In order to analyze the effect of cyclic loading on the bond behavior of samples, six different classes of strengthening systems have been selected, with the aim of covering at best the range of currently available FRCM applications.

FRCM strengthening systems tested include bidirectional carbon, glass, aramid-glass and basalt grids, made of dry or coated fibers and applied in some cases with an adhesion promoter.

This research aims at improving the knowledge about the use of FRCM composites for the strengthening of masonry structures by collecting a wide database of experimental results useful for characterizing the monotonic and cyclic bond behavior of this class of strengthening systems.

2. MATERIALS, TEST SET-UP AND INSTRUMENTATIONS

The experimental campaign here described focuses on the investigation of the effects given by cyclic loading on the bond behavior of several types of FRCM strengthening systems applied to masonry elements. To this purpose, the experimental work aimed at investigating three main aspects: mechanical properties of the different FRCM composite materials, FRCMs-masonry bond behavior under monotonic and cyclic loading.

2.1. Materials properties and samples preparation

Specimens used as masonry substrate were built by using five clay bricks (with standard dimensions of 250×120×55 mm^3) and a commercial lime mortar of limited performances, adopting mortar joints about 10 mm thick. Bricks used for masonry panels preparation were new clay bricks

produced by compaction, similarly to ancient bricks, and not by extrusion (which is the most common actual process).

Bricks compressive strength was evaluated along different principal directions, in particular perpendicular (⊥) and parallel (//) to the bed face [20,22], by means of cylindrical samples with 50 mm diameter and the same height core-drilled from the bricks, obtaining respectively 18.60 and 23.05 MPa. Bricks tensile strength along the same directions was also investigated, by using two different methods: brick flexural strength ($f_{t,\ flex}$) was determined on prismatic samples (with dimensions 40×40×240 mm^3) subjected to three-point bending tests, whereas brick splitting tensile strength ($f_{t,\ split}$) was determined on core-drilled cylindrical samples by means of the Brazilian splitting test.

Flexural strength ($f_{t,\ flex}$) and compressive strength (f_c) of mortar used for masonry panels realization (NHL_j) was measured according to [52]. All the results are reported in Table 1.

The strengthening systems tested considered grids made of glass, aramid-glass, basalt and carbon fibers applied, as externally bonded reinforcements, through different natural hydraulic lime (NHL) mortars. They were components of commercially available strengthening systems coming from different producers. The choice of using different types of reinforcement was aimed at investigating possible different behaviors related to materials and was intended to provide for an extended overview of the effect of cyclic loading on FRCM strengthened structural elements.

The six different types of textiles used for the strengthening systems are described in the following:

- Carbon C1 was an uncoated carbon fiber grid, characterized by a nominal spacing of 9 mm and a density of 170 g/m^2 (equivalent thickness = 0.047 mm). Tensile strength and elastic modulus were, respectively, 2200 MPa and 240 GPa (producer data). This grid was embedded inside the mortar with the addition of an adhesion promoter, which was used to improve fibers-matrix adhesion. Its application was previously investigated on similar samples [30,31], highlighting significant improvement of the adhesion between fibers and

matrix, limiting the possible slip between the different layers and allowing obtaining sensibly higher maximum loads.

- Carbon C2 was a dry carbon fibers grid with a spacing of 20 mm and a density of 170 g/m^2 (equivalent thickness 0.047 mm). Tensile strength and elastic modulus were, respectively, 1900 MPa and 240 GPa (as specified by the producer).
- Glass G1 was an uncoated glass fibers grid with a strand spacing of 12 mm and a density of 300 g/m^2 (equivalent thickness = 0.060 mm). This grid was embedded inside the mortar with the addition of the same adhesion promoter used for carbon C1. Tensile strength and elastic modulus specified by the producer were, respectively, 1000 MPa and 65 GPa.
- Glass G2 was a coated glass fibers grid with a nominal strand spacing of 25 mm and a density of 225 g/m^2 (equivalent dry fibers thickness of 0.035 mm). Tensile strength and elastic modulus specified by the producer were, respectively, 1285 MPa and 72 GPa.
- Aramid-glass AG1 was an aramid-glass fiber grid with a nominal spacing of 15 mm and a density of 250 g/m^2 (equivalent dry fibers thickness of 0.031 mm). Tensile strength and elastic modulus specified by the producer were, respectively, 1600 MPa and 110 GPa.
- Basalt B1 was a basalt grid with a nominal strand spacing of 9 mm and a density of 260 g/m^2 (equivalent thickness of 0.049 mm). Tensile strength and elastic modulus specified by the producer were, respectively, 1700 MPa and 70 GPa.

The coupling between different grids and mortars ($NHL_{str,i}$) is reported in Table 2. Table 1 shows the mechanical properties of the different mortars used for strengthening. They were obtained through the same tests previously described for the characterization of NHL_j. Six different strengthening systems were subject to experimental tests according to Table 3. All the specimens for all the tests types were prepared by using the same materials and the same geometry, in order to be able to compare experimental outcomes.

Geometry and other details of the prepared specimens can be seen in Figure *1a* for the tensile test and in Figure 1*b* for the bond test. The reinforcement width was chosen as an integer multiple of the

grid spacing and including at least 4 bundles, so as to make the samples more representative of the real system. The adopted reinforcement widths (*w*) are reported in Table 2. For all the specimens, the global mortar thickness was 6 mm, with the grid inside, and it was controlled by making use of appropriate spacers.

Preparation of all samples subjected to bond tests was done without any particular masonry surface preparation, but only following a standard procedure including brushing, cleaning and wetting of the surface before applying the first matrix layer. A bond length (*BL* in Figure 1*b*) of 260 mm was chosen for all the samples subject to bond tests, after adopting an unbonded length (*UL*) of 30 mm, measured from the front side of the sample. The unbonded part of the reinforcement was impregnated with epoxy resin in order to promote a good transverse load redistribution.

In case of C1 and G1 samples, for both tensile and bond tests, the adhesion promoter was applied over the first matrix layer, before placing the textile, and then above the reinforcement grid, before applying the second matrix layer.

2.2. Experimental set-up for tensile tests

Tensile tests were performed by using a servohydraulic testing machine with hydraulic wedge grips (maximum capacity 100 kN). Before the tests, specimen ends were strengthened by using composite tabs (Figure 1*a*), in order to avoid local failure due to grip clamping. The use of the hydraulic clamping system allowed to choose an appropriate pressure in order to avoid slipping phenomena and, at the same time, prevent damage to the sample.

Tensile tests were carried out under displacement control, with a rate of 0.1 mm/min during the first un-cracked phase, which was then increased to 0.2 mm/min during the cracked phase. The applied load was measured by means of the onboard class 0.5 load cell, while the sample deformation was measured thanks to an axial extensometer, using a gage length (*GL* in Figure 1*a*) of 200 mm.

The experimental set-up is shown in Figure 2*a*.

2.3. Experimental set-up for single-lap shear tests

The experimental set-up adopted for single-lap shear tests, which was validated during several experimental campaigns performed on FRP and FRCM composite materials applied on masonry elements [32,34,35,53], is composed by a rigid steel frame, fixed on the hydraulic wedge grips of the same servohydraulic testing machine used for tensile tests at the bottom (see Figure 2*b*). The loaded end of the FRCM reinforcement was impregnated with epoxy resin, in order to promote a good redistribution of the force applied by the testing machine among the different bundles and then was strengthened making use of FRP tabs.

Force was measured by using the onboard class 0.5 load cell, while the relative displacement (slip) between fibers and substrate was measured by means of two 20 mm LVDTs. In more detail, the two displacement transducers were fixed on the substrate by means of appropriate holder glued on masonry and placed in contrast with an omega-shaped aluminum profile glued to the first cross-section of the FRCM unbonded part (see Figure 1*b* and 2*b*).

All the bond tests were performed under displacement control; monotonic tests were characterized by a rate of 0.15 mm/min. Cyclic tests were always in traction, which means without force reversal; 5 cycles were done for three growing load levels (25, 50 and 75% of the average peak load registered during monotonic tests) before the maximum load, at a rate of 0.15 mm/min during the loading phase and allowing a maximum speed of 0.5 mm/min during the unloading phase. Most of the cases were characterized by sudden delamination/failure at peak, thus preventing the realizations of cycles during the delamination phase.

3. EXPERIMENTAL RESULTS

3.1. Tensile tests

Table 4 shows the failure modes of all the samples tested and the key parameters (stress, strain, elastic moduli) defining the different phases of the stress-strain curves identified during tensile tests

and characterizing their tensile behavior. All the stresses were evaluated by taking into account the dry fibers cross-section only.

The two identified failure mechanisms were: (A) fiber rupture within the gage length of the mechanical extensometer or (B) tensile failure outside the gage length (see Figure 3).

C1 samples (Figure 4*a*) showed a trilinear behavior with smooth transitions between the different phases: after the first branch (un-cracked phase), where all the cross-section of the specimen is effective, cracking occurred, with the formation of a relevant number of cracks characterized by a very reduced width, progressively increasing in number along the sample (second phase) and leading to the tensile rupture of the fibers in correspondence of one of the previously opened cracks at the end of the third and final branch. The presence of the adhesion promoter makes the transition between the different branches very smooth and the resulting experimental outcomes are very repeatable, with a reduced scattering. Similarity between third branch elastic modulus (E_3) and that of dry fibers confirms that, during this phase, specimen behavior was mainly affected by the presence of the reinforcement grid.

C2 samples showed instead more scattered results, with a significant reduction in stiffness after the formation of the first crack which appeared at the end of the first linear branch (Figure 4*b*). During the cracked phase, a progressive growing of few visible cracks was observed, with a relevant fiber slippage and sometimes mortar disaggregation, until final failure. For this reason, it was difficult to properly locate the end of the second branch, the second key point, which was not reported in Table 4, and the elastic modulus E_3 has a certain degree of uncertainty.

Figure 4*c* shows the tensile behavior of G1 specimens: this type of FRCM showed, unlike C1 carbon samples, a typical bilinear behavior, where, after the first un-cracked phase, only a single almost linear final branch was identified. The application of an adhesion promoter led to the formation of widespread micro-cracks, as for C1 samples, with the overall tensile behavior characterized by a progressive transition between the un-cracked and the cracked phase. The extremely reduced crack widths identified during the tensile tests performed on C1 and G1 samples

can be explained by assuming that the action of the matrix and of the adhesion promoter, in particular, was really effective in redistributing load and preventing fiber slippage.

Cyclic tensile tests performed on C1 and G1 strengthening systems [31] showed no reduction in the maximum load and no significant variation on the tensile behavior of the samples after cyclic loading, in comparison to standard monotonic tests, indicating however that cyclic tests can be useful in order to evaluate residual deformation and to better evaluate the behavior of the samples.

G2 specimens showed a bilinear behavior (see Figure 4*d*), with a smooth transition between the first and the second branch and a reduced scattering of results for what concerns ultimate stress and elastic moduli. Their tensile behavior, similar to that from G1 samples, may be attributed to the addition of short fibers inside the mortar matrix, which seems very effective, during the second (cracked) phase, in reducing cracks width and preventing the formation of the corresponding load drops in stress-strain graph.

The tensile behavior of AG1 samples was quite different from that of the other FRCM strengthening systems (Figure 4*e*), showing, after the first branch, the formation of an evident crack in the central part of the sample and few (one or two) other cracks during the last (cracked) phase. Since for this group of reinforcement it is not possible to properly define a second branch, elastic moduli reported in Table 4 are calculated along the first linear branch (E_1), after which a remarkable reduction in stiffness was recorded, and along the last cracked phase (E_3). Despite this particular behavior, stress-strain graphs show a reduced scattering in terms of ultimate stress at failure.

Basalt (B1) specimens showed a trilinear behavior, with a clear distinction between the different phases (see Figure 4*f*). In fact, after the first linear branch, the second (cracking) phase started, with the formation of three or four distributed cracks along the extensometer gage length, before the beginning of the third phase, where cracks progressively increased their width, until the tensile failure of the textile.

3.2. Bond tests

In the following, failure modes, maximum capacity and stress-slip curves will be presented and discussed for the six different FRCM types tested, for both monotonic and cyclic single-lap shear tests.

As previously discussed, slip was evaluated as the relative displacement between the first section of the unbonded part of the reinforcement and the adjacent substrate through direct displacement transducers (LVDTs) readings.

Table 5 shows bond capacity of the samples tested, together with the identified failure modes and the comparison between monotonic and cyclic tests results.

3.2.1 *Failure modes*

Bond failure modes are described in this section by referring to the classification reported in [54] and those observed are presented in Figure 5.

Failure mode C (see Figure 5*a*) is typical of C1 samples, where carbon grid was applied with an adhesion promoter; in more detail, failure occurred due to delamination located within the inner mortar layer, with the detachment of the upper matrix layer together with the carbon textile and only a thin layer of mortar coming from the lower matrix layer. The identified failure mechanism is typical of carbon FRCM with a proper adhesion between fibers and matrix and seems related to the use of an adhesion promoter, which proved to be effective in limiting fiber slippage [30]. The detached layer of matrix is not regular and evident variations in thickness can be identified in presence of the mortar joints of the underlying substrate and within the voids of the reinforcement grid (thicker layer). Bond capacity seems limited, in this case, to the maximum shear strength of the matrix used within the FRCM. This failure mode characterized all the monotonic and cyclic bond tests performed on this group of reinforcement.

C2 carbon samples, where an uncoated reinforcement grid was used, showed, as expected, a significantly different bond behavior characterized by an evident slippage of the fibers within the

matrix (see Failure mode D in Figure 5*b*). This failure mode, detected both on monotonic and cyclic tests performed on C2 carbon samples, also occurred during some monotonic bond tests on B1 basalt fiber (see Table 5).

A different failure mode, where fiber slippage ended with the rupture of the FRCM grid (see Failure mode D** in Figure 5c) was detected on G2 glass samples, which have an external coating on the fibers. The choice of performing bond tests on these groups of samples was made with the purpose of evaluating their possible different mechanical behavior if compared, for example, to G1 specimens, where dry glass fibers are coupled with an adhesion promoter.

In fact, this FRCM group (G1), where the adhesion promoter proved to be very effective [26], showed, as recurring failure mechanism, the tensile failure of the reinforcement grid at the beginning of the bonded part. This failure mechanism is typical of glass grids where a proper adhesion between matrix and substrate is guaranteed and occurred with the progressive fraying of the fibers which led to the final tensile failure of the yarns.

The same failure mode was detected on monotonic and cyclic bond tests performed on aramid-glass samples (AG1) and, in this particular case, systematically occurred in correspondence of the first transversal bundle (see Failure mode E in Figure 5*d*).

A slightly different mechanism, where a partial delamination of the FRCM reinforcement occurred at the beginning of the bonded area before fiber rupture (see Failure mode E* in Table 5), was detected in some G1 and B1 samples, where probably bond capacity was weaker.

The bond behavior identified for the different classes of FRCM systems show that fiber rupture is the most common mechanism for glass and basalt samples, leading to an high exploitation of their tensile capacity, whereas carbon fibers are unable to reach their maximum tensile strength without manifesting premature delamination or slippage phenomena. In this framework, single lap shear tests proved to be particularly useful for evaluating failure modes and maximum capacity of the strengthening systems when applied on masonry substrate, which can be very different from those emerging from tensile tests.

3.2.2 *Monotonic bond behavior: stress-slip curves and maximum bond capacity*

The monotonic bond behavior of the considered FRCM systems is presented in Figure 6, whereas their average maximum bond capacity and its statistical variation, for both monotonic and cyclic tests (described in the following), are reported in Table 5. Consistently with tensile tests, even for direct shear tests, the stress refers to the dry fibers cross-section only; in this way, tensile and bond tests results can be directly compared. An efficiency parameter, η, calculated as the ratio between the maximum stress registered during bond and tensile tests, respectively, has been also taken into account (see Table 5) for comparing and discussing the load capacity of the systems subjected to the two different mechanical characterization methods.

The maximum load registered during bond tests performed on C1 samples showed a reduced statistical variation (CoV < 6%). All the samples, as already discussed, showed the same failure modes: full delamination within the lower matrix layer with a repeatable behavior (see Figure 6*a*). In more detail, the bond behavior of this FRCM type was defined by a first almost linear phase and a following non-linear subhorizontal behavior, which started after the starting of delamination and continued until the complete detachment of the reinforcement.

C2 specimens showed a repeatable behavior, providing for a very limited statistical variation (CoV < 4% in monotonic tests), but also low ultimate stresses. In fact, after a first almost linear branch, the peak was soon reached through an important slippage (Figure 6*b*). After the maximum force, a progressive softening branch can be observed, with a growing fiber slippage and sometimes also with fiber damage leading to a reduced residual load, due to friction effect between dry carbon fibers and matrix. The identified behavior suggested that the transversal yarns of the textile could be not completely efficient since, after the rupture of the connections between the dry carbon fibers, they showed little importance in preventing longitudinal bundles slippage.

The bond behavior of G1 samples was found to be very different from that observed on carbon samples (Figure 6*c*): in fact, after the first almost linear branch, an abrupt failure or a reduced

subhorizontal curve, occurring during the tensile rupture of the glass grid, can be identified (Failure mode E), sometimes with a partial delamination (Failure mode E* in Table 5).

Figure 6*d* shows the three stress-slip curves registered during monotonic bond tests on G2 samples: they were characterized by a nonlinear behavior that started almost from the beginning, with the first knee point, where the early fiber slippage started, clearly identifiable in the graph. After the peak, a sudden tensile failure of the reinforcement grid occurred, without a post-peak significant residual bond capacity (Failure mode D**). In more detail, fiber slippage started early before the peak and significantly increased after the rupture of the connections between longitudinal and transversal bundles, leading to a remarkable deformability of the system. In this case, as for C2 carbon specimens, the transversal bundles seem not completely efficient to prevent the slippage of the longitudinal yarns. The reasons behind this particular behavior were properly investigated and explained in [53].

Aramid-glass samples, instead, showed (Figure 6*e*) a bond behavior which seems in many aspects similar to that observed on G1 specimens. The matrix capacity and the good connections between longitudinal and transversal bundles, were efficient in preventing fiber slippage and led to a high exploitation of the reinforcement tensile capacity. In fact, all the tests ended with a sudden failure of the composite grid, as showed in stress-slip curves reported in Figure 6*e*. As previously discussed, for this class of strengthening systems, tensile failure was identified in correspondence of the first transversal bundle (see Figure 5*d*). Maximum bond capacity registered in monotonic bond tests is affected by a very reduced statistical variation (CoV < 2%).

Basalt samples, despite a common first nonlinear phase (Figure 6*f*), showed two different behaviors, according to the different failure modes detected (see Table 5): fiber slippage (D) or tensile failure of the composite grid outside of the bonded area, sometimes with partial delamination at the beginning of the bonded region (Failure mode E and E*). In the first case, after the peak, a significant load drop with a negligible residual bond capacity (specimens B1_1 and B1_2) can be

identified; in the second case, after the maximum load, a limited sub-horizontal delamination plateau, where a progressive fraying of the basalt fiber occurred, can be observed (sample B1_3).

The efficiency parameter η reported in Table 5 show that, in general, glass and basalt samples are able to achieve a high exploitation of their maximum tensile capacity, whereas lower values can be expected for high performance fibers (such as carbon fibers). The particular behavior of C2 carbon samples, where fiber slippage occurred at very low load levels, can be explained considering the lack of an adhesion promoter or fiber coating in this strengthening system, which caused a poor adhesion between the reinforcement grid and the matrix.

3.3. Cyclic bond tests

The effects of cyclic loading on the bond behavior of FRCM specimens, in terms of maximum capacity, bond behavior and cyclic degradation will be analyzed and discussed in this section.

3.3.1 *Effects of cyclic loading on failure modes*

Table 5 shows the failure modes detected during both monotonic and cyclic bond tests. The effect of cyclic loading on the failure mode of the samples appeared rather limited, even if in basalt specimens cycles repetition often led to more brittle failure modes, due to energy dissipation through cycles. In fact, during cyclic tests, Failure mode D detected during monotonic tests disappeared and, after the first nonlinear phase, only Failure modes E and E*, characterized by the final tensile failure of the composite grids, occurred.

3.3.2 *Effects of cyclic loading on bond capacity and on the stress-slip behavior*

Bond tests results reported in Table 5 show how cyclic loading affects maximum bond capacity: the small variations detected shifting from monotonic to cyclic direct shear tests (< 7%) allow to conclude that it is not possible to identify a significant influence of cyclic loading performed at relevant stress levels on maximum forces, at least for a low number of cycles (5 repetitions for each of the three predefined load levels). In fact, average ultimate stresses recorded during monotonic

and cyclic bond tests, always characterized by a reduced statistical variation, were absolutely comparable and didn't show any sensitivity to the type of loading.

A graphical comparison between the global stress-slip behavior of carbon, glass, aramid-glass and basalt FRCM samples subjected to monotonic and cyclic bond tests is shown in Figure 7*a-f*, respectively, where curves coming from cyclic tests were over-imposed to the envelopes (gray areas) obtained from monotonic tests. Some common features can be found irrespective of the type of FRCM: load cycles repetition produces an increase of slip growing with the applied stress level; the cyclic stress-slip envelope matches quite accurately the monotonic envelope. This is possible since the slope of the loading-unloading branches is locally higher than that of the monotonic envelope at the same stress level; only after exceeding the previous stress level, a nonlinear behavior can be observed with a progressive slope reduction leading to the monotonic envelope. Cycle after cycle, the slip increment is reduced, suggesting a stabilization of the process (Figure 8).

For C1 carbon samples (Figure 7*a*), it was possible to impose load cycles even during the delamination process, where an increase of slip was observed due to the bond deterioration related to cycles. Even in this case, the wavy shape of the plateau was observed. Results from C2 samples (Figure 7*b*), showed that even cycles imposed along the softening branch were not able to remarkably move the curve from the monotonic envelope.

For all the others FRCM materials, the fiber rupture was brittle and load cycles during the delamination phase were not possible. Slips at peak remained substantially unchanged, suggesting that for this type of failure cycles didn't increase the deformability.

3.3.3 *Cyclic slip increment*

In order to properly analyze the cycle-by-cycle slip variation in correspondence of the same load level, the relative slip increment Δ was defined as:

$$\Delta_i = \frac{s_{i+1} - s_i}{s_2 - s_1}, \qquad i = 1, 2, 3, 4 \tag{1}$$

where s_i and s_{i+1} are peak slip values registered along two subsequent cycles performed at the same assigned load level, whereas s_1 and s_2 are the peak slip values recorded, respectively, during the first and the second cycle (see Figure 8). The evaluation of the general slip increment (s_{i+1}-s_i) with respect to the first one (s_2-s_1), allowed the comparison between increments coming from different stress levels. The results obtained for carbon, glass, aramid-glass and basalt specimens are reported in Figure 9*a-d*, respectively, where a single curve for each assigned load level is shown. Since for each FRCM strengthening system at least 3 tests were performed, the reported curves have to be considered as averages between tests repetitions.

The graphs showed a specific and repeatable behavior, with an evident slip increment reduction when performing growing number of cycles, according to a nonlinear behavior. In general, this trend of reduction is greater at lower stress levels, suggesting that higher stress levels introduce, as expected, larger irreversible slippage. The number of cycles performed (5) doesn't allow to draw some general conclusions about this aspect; nevertheless, these quantities can be considered as realistic values of cycles requested at this so high stress level by a relevant earthquake.

4. CONCLUSIONS

Results of tensile tests and of monotonic and cyclic bond tests carried out on six different types of FRCMs are presented and discussed in this paper. FRCM composites tested here are based on bidirectional carbon, glass, aramid-glass and basalt grids applied with 5 different types of NHL based matrices and, in two cases, with an adhesion promoter. Strengthening systems were selected with the purpose of covering the most extensive possible scenario, allowing for the observation of different failure mechanisms, tensile and bond behaviors.

Tensile characterization of strengthening systems was performed in order to define the main mechanical parameters (stress, strain, elastic moduli) needed for a proper definition of simplified trilinear or bilinear constitutive laws.

Single-lap shear tests performed after applying the reinforcements on masonry substrate showed a wide scenario of failure modes, depending on the reinforcement grid type and geometry, on matrix

properties and on the possible application of an adhesion promoter: matrix delamination, fiber slippage or grid tensile failure, with some interactions between the different mechanisms. In some cases, different bond behaviors have to be attributed to the effectiveness of the grid transversal bundles, which can lead to the tensile failure of the reinforcement or simply break and then slip with respect to the longitudinal yarns. The application of the adhesion promoter proved its effectiveness when applied on dry fibers as an alternative to external coating. Stress-slip curves obtained from bond tests were analyzed and discussed, highlighting similarities and differences on the bond behavior of samples that led to the identified failure mechanisms.

Single lap shear tests proved to be very helpful for evaluating failure mechanisms and maximum capacity of FRCM systems, also in comparison to direct tensile tests: results show high exploitation ratios for glass and basalt samples and reduced performances of carbon fibers if not coupled with external coating or surface treatments for improving adhesion.

Cyclic loading seemed to have negligible influence on the maximum bond capacity, but cycles repetition, however, allowed to evaluate cyclic degradation and residual slips.

The repetition of cycles performed at the same load level during the first phase of bond tests pointed out an evident slip variation between the first and the second cycle, with a progressive attenuation among cycles. Bond degradation, in general, does not prevent, however, to reach the monotonic envelope during the following loading phase. In basalt samples, cyclic loading was found to slightly change the failure mechanism, often leading to more brittle failure modes after the peak load, probably because of energy dissipation through loading-unloading cycles.

The introduction of a simple discrete parameter (Δ) evaluated for each cycle repetition led to a quantitative estimation of cyclic degradation stabilization.

Cyclic loading performed after the peak load, such as in carbon samples which manifested matrix delamination, highlighted that repetition of cycles after the onset of delamination process progressively deteriorates the bond capacity allowing delamination propagation along the FRCM composite, without however having a clear influence on the maximum load. In general, application

of load cycles didn't remarkably affect the performances of the FRCM system, proving their reliability under seismic forces also.

Experimental outcomes provided useful information about the cyclic behavior of strengthening systems, highlighting that capacity reduction after cycles repetition is not relevant and confirming that traditional monotonic tests can be used for the materials qualification procedure, as suggested by the most recent guidelines [11].

Further studies are currently in progress, also on large-scale reinforced elements, to confirm this behavior and to draw final conclusions.

5. ACKNOWLEDGEMENTS

The financial support of (Italian) Department of Civil Protection (ReLUIS 2019 Grant – Innovative Materials) is gratefully acknowledged. The authors would like also to thank Fibrenet S.p.A., G&P Intech S.r.l., Mapei S.p.A., Kerakoll S.p.A. and Fassa S.r.l for providing materials.

REFERENCES

[1] Triantafillou TC. Composites: a new possibility for the shear strengthening of concrete, masonry and wood. Compos Sci Technol 1998;58:1285-1295.

[2] Triantafillou T, Papanicolaou C. Innovative applications of textile-based composites in strengthening and seismic retrofitting as well as in the prefabrication of new structures. Adv Mater Res 2013;639-640:26-41.

[3] Angelillo M, Babilio E, Cardamone L, Fortunato A, Lippiello M. Some remarks on the retrofitting of masonry structures with composite materials. Compos Part B 2014;61:11-16.

[4] Rousakis TC. Reusable and recyclable nonbonded composite tapes and ropes for concrete columns confinement. Compos Part B 2016;103:15-22.

[5] Hollaway LC, Teng JG. Strengthening and rehabilitation of civil infrastructures using fibre-reinforced polymer (FRP) composites, vol. 25. Cambridge, England: Woodhead Publishing Limited, Great Abington, 2008.

[6] Fardis MN. Seismic design, assessment and retrofitting of concrete buildings. London New York: Springer, Dordrecht Heidelberg, 2009.

[7] Rousakis TC. Inherent seismic resilience of RC columns externally confined with nonbonded composite ropes. Compos Part B 2018;135:142-148.

[8] Butler M, Mechtecherine V, Hempel S. Durability of textile reinforced concrete made with AR glass fibre: effect of matrix composition. Mater Struct 2010;43:1351-1368.

[9] AC 434. Acceptance criteria for masonry and concrete strengthening using Fabric-Reinforced Cementitious Matrix (FRCM) composite systems. 2013.

[10] ACI 549.4R-13. Guide to design and construction of externally bonded Fabric-Reinforced Cementitious Matrix (FRCM) systems for repair and strengthening concrete and masonry structures. 2013.

[11] CNR-DT 215/2018. Istruzioni per la progettazione, l'esecuzione ed il controllo di interventi di consolidamento statico mediante l'utilizzo di compositi fibrorinforzati a matrice inorganica. 2018. [in Italian].

[12] Capozucca R. Experimental FRP/SRP-historic masonry delamination, Compos Struct 2010;92:891-903.

[13] Capozucca R. Effects of mortar layers in the delamination of GFRP bonded to historic masonry. Compos Part B 2013;44:639-649.

[14] Carloni C, Subramaniam KV. FRP–masonry debonding: numerical and experimental study of the role of mortar joints. J Compos Constr 2012;16(5):581-589.

[15] Carrara P, Ferretti D, Freddi F. Debonding behavior of ancient masonry elements strengthened with CFRP sheets, Compos Part B 2013;45:800-810.

[16] Valluzzi MR, Oliveira DV, Caratelli A, Castori G, Corradi M, de Felice G, Garbin E, Garcia D, Garmendia L, Grande E, Ianniruberto U, Kwiecień A, Leone M, Lignola GP, Lourenço PB, Malena M, Micelli F, Panizza M, Papanicolau CG, Prota A, Sacco E, Triantafillou TC,

Viskovic A, Zając B, Zuccarino G. Round Robin Test for composite-to-brick shear bond characterization. Mater Struct 2012;45(12):1761-1791.

[17] de Felice G, Aiello MA, Bellini A, Ceroni F, De Santis S, Garbin E, Leone M, Lignola GP, Malena M, Mazzotti C, Panizza M, Valluzzi MR. Experimental characterization of composite-to-brick masonry shear bond, Mater Struct 2016;49:2581-2596.

[18] Kwiecień A, de Felice G, Oliveira DV, Zając B, Bellini A, De Santis S, Ghiassi B, Lignola GP, Lourenço PB, Mazzotti C, Prota A. Repair of composite-to-masonry bond using flexible matrix. Mater Struct 2016;49:2563-2580.

[19] Mazzotti C, Ferracuti B, Bellini A. Experimental bond tests on masonry panels strengthened by FRP. Compos Part B 2015;80:223-237.

[20] Mazzotti C, Sassoni E, Bellini A, Franzoni E. Strengthening of masonry elements by FRP: Influence of brick mechanical and microstructural properties. Key Eng Mater 2015;624:330-337.

[21] Mazzotti C, Ferracuti B, Bellini A. Experimental study on masonry elements strengthened by GFRP: the role of inclination between mortar joints and GFRP sheets. Key Eng Mater 2015;624:559-566.

[22] Sassoni E, Andreotti S, Bellini A, Mazzanti B, Bignozzi MC, Mazzotti C, Franzoni E. Influence of mechanical properties, anisotropy, surface roughness and porosity of brick on FRP debonding force. Compos Part B 2017;108:257-269.

[23] Sassoni E, Sarti V, Bellini A, Mazzotti C, Franzoni E. The role of mortar joints in FRP debonding from masonry. Compos Part B 2018;135:166-174.

[24] Ceroni F, Leone M, Rizzo V, Bellini A, Mazzotti C. Influence of mortar joints on the behaviour of FRP materials bonded to different masonry substrates. Eng Struct 2017;153:550-568.

[25] Bellini A, Mazzotti C. A review on the bond behavior of FRP composites applied on masonry substrates. RILEM Technical Letters 2017;2:74-82.

[26] Ceroni F, de Felice G, Grande E, Malena M, Mazzotti C, Murgo F, Sacco E, Valluzzi MR. Analytical and numerical modeling of composite-to-brick bond. Mater Struct 2014;47(12):1987-2003.

[27] De Santis S, de Felice G. Tensile behaviour of mortar-based composites for externally bonded reinforcement systems. Compos Part B 2015;68:401-413.

[28] D'Ambrisi A, Feo L, Focacci F. Experimental and analytical investigation on bond between Carbon-FRCM materials and masonry. Compos Part B 2013;46:15-20.

[29] de Felice G, De Santis S, Garmendia L, Ghiassi B, Larrinaga P, Lourenço PB, Oliveira DV, Paolacci F, Papanicolaou CG. Mortar-based systems for externally bonded strengthening of masonry. Mater Struct 2014;47(12):2021-2037.

[30] Bellini A, Ferracuti B, Mazzotti C. Effect of matrix on bond between FRCM and masonry. Proc. of FRPRCS-12 & APFIS-2015 Joint Conference, Nanjing, China, 14-16 December 2015.

[31] Bellini A, Mazzotti C. Bond behavior and tensile properties of FRCM composites applied on masonry panels. Proceedings of the 10th International Conference on Structural Analysis of Historical Constructions - SAHC 2016, Leuven, Belgium, 13 - 15 September 2016. p. 322-329.

[32] Carozzi FG, Bellini A, D'Antino T, De Felice G, Focacci F, Hojdys L, Laghi L, Lanoye E, Micelli F, Panizza M, Poggi C. Experimental investigation of tensile and bond properties of Carbon-FRCM composites for strengthening masonry elements. Compos Part B 2017;128:100-119.

[33] Caggegi C, Carozzi FG, De Santis S, Fabbrocino F, Focacci F, Hojdys L, Lanoye E, Zuccarino L. Experimental analysis on tensile and bond properties of PBO and aramid fabric reinforced cementitious matrix for strengthening masonry structures. Compos Part B 2017;127:175-195.

[34] De Santis S, Ceroni F, de Felice G, Fagone M, Ghiassi B, Kwiecień A, Lignola GP, Morganti M, Santandrea M, Valluzzi M, Viskovic A. Round Robin Test on tensile and bond behavior of Steel Reinforced Grout systems. Compos Part B 2017;127:100-120.

[35] Leone M, Aiello MA, Balsamo A, Carozzi FG, Ceroni F, Corradi M, Gams M, Garbin E, Gattesco N, Krajewski P, Mazzotti C, Oliveira D, Papanicolaou C, Ranocchiai G, Roscini F, Saenger D. Glass fabric reinforced cementitious matrix: tensile properties and bond performance on masonry substrate. Compos Part B 2017;127:196-214.

[36] Lignola GP, Caggegi C, Ceroni F, De Santis S, Krajewski P, Lourenço PB, Morganti M, Papanicolaou C, Pellegrino C, Prota A, Zuccarino L. Performance assessment of Basalt FRCM for retrofit applications on masonry. Compos Part B 2017;128:1-18.

[37] Bellini A, Incerti A, Mazzotti C. Out-of-plane behavior of masonry walls strengthened by FRCM composites. Proceedings of the 10th International Conference on Structural Analysis of Historical Constructions - SAHC 2016, Leuven, Belgium, 13 - 15 September 2016. p. 1053-1060.

[38] Bellini A, Incerti A, Mazzotti C. Out-of-plane strengthening of masonry walls with FRCM composite materials. Key Eng Mater 2017;747:158-165.

[39] Bellini A, Incerti A, Bovo M, Mazzotti C. Effectiveness of FRCM reinforcement applied to masonry walls subject to axial force and out-of-plane loads evaluated by experimental and numerical studies. Int J Archit Herit 2018;12(3):376-394.

[40] Murgo FS, Mazzotti C. Masonry columns strengthened with FRCM system: Numerical and experimental evaluation. Constr Build Mater 2019;202:208-222.

[41] Incerti A, Tilocca AR, Ferretti F, Mazzotti C. Influence of masonry texture on the shear strength of FRCM strengthened masonry panels. Proceedings of the 11th International Conference on Structural Analysis of Historical Constructions - SAHC 2018, Cusco, Perù, 11 - 13 September 2018. p. 1623-1631.

[42] Zhu D, Peled A, Mobasher B. Dynamic tensile testing of fabric-cement composites. Constr Build Mater 2011;25:385-395.

[43] Contamine R, Si Larbi A, Hamelin P. Contribution to direct tensile testing of textile reinforce concrete (TRC) composites. Mat Sci Eng A 2011;528:8589-98.

[44] Arboleda D, Carozzi FG, Nanni A, Poggi C. Testing procedures for the uniaxial tensile characterization of fabric-reinforced cementitious matrix composites. J Compos Constr 2016; 20(3). ASCE, 04015063.

[45] Carozzi FG, Poggi C. Mechanical properties and debonding strength of Fabric Reinforced Cementitious Matrix (FRCM) systems for masonry strengthening. Compos Part B 2015;70:215-230.

[46] Hegger J, Will N, Bruckermann O, Voss S. Load bearing behavior and simulation of textile reinforced concrete. Mater Struct (RILEM) 2006;39(8):765-76.

[47] Raupauch M, Orlowsky J, Buttner T, Dilthey U, Schleser M. Epoxy-impregnated textiles in concrete – load bearing capacity and durability. ICTRC 2006:77-88.

[48] D'Antino T, Carloni C, Sneed LH, Pellegrino C. Matrix–fiber bond behavior in PBO FRCM composites: a fracture mechanics approach. Eng Fract Mech 2014;117:94-111.

[49] D'Ambrisi A, Feo L, Focacci F. Experimental analysis on bond between PBO-FRCM strengthening materials and concrete. Compos Part B 2013;44(1):524-532.

[50] D'Ambrisi A, Feo L, Focacci F. Experimental and analytical investigation on bond between Carbon–FRCM materials and masonry. Compos Part B 2013;46:15-20.

[51] de Felice G, De Santis S, Garmendia L, Ghiassi B, Larringa P, Lourenço PB, Oliveira DV, Paolacci F, Papanicolau CG. Mortar-based systems for externally bonded strengthening of masonry, Mater Struct 2014;47(12):2021-2037.

[52] UNI-EN 1015-11. Methods of test for mortar for masonry – Part 11: determination of flexural and compressive strength of hardened mortar. 2007.

[53] Bellini A, Bovo M, Mazzotti C. Experimental and numerical evaluation of fiber-matrix interface behaviour of different FRCM systems. Compos Part B 2019;161:411-426.

[54] Ascione L, de Felice G, De Santis S. A qualification method for externally bonded Fibre Reinforced Cementitious Matrix (FRCM) strengthening systems. Compos Part B 2015;78:497-506.

Table 1. Materials mechanical characterization.

Sample type	Compressive strength f_c [MPa]	Flexural strength $f_{t,flex}$ [MPa]	Splitting tensile strength $f_{t,split}$ [MPa]
Brick (⊥ bed)	18.60	4.65	2.60
Brick (∥ bed)	23.05	4.84	3.15
NHL_j mortar	4.18	1.87	-
$NHL_{str,1}$ matrix	9.83	3.84	-
$NHL_{str,2}$ matrix	16.07	5.82	-
$NHL_{str,3}$ matrix	14.74	5.88	-
$NHL_{str,4}$ matrix	13.81	3.27	-
$NHL_{str,5}$ matrix	20.44	5.75	-

Table 2. FRCM components and their coupling.

Sample type	Reinforcement grid	Matrix	Reinforcement width w [mm]	Number of strands
C1	Carbon C1	$NHL_{str,1}$	54	6
C2	Carbon C2	$NHL_{str,2}$	80	4
G1	Glass G1	$NHL_{str,1}$	60	5
G2	Glass G3	$NHL_{str,3}$	100	4
AG1	Aramid-glass AG1	$NHL_{str,4}$	75	5
B1	Basalt B1	$NHL_{str,5}$	65	7

Table 3. Experimental plan.

Sample type	Tensile tests	Bond tests	
		Monotonic	Cyclic
C1 (carbon)	5	5	5
C2 (carbon)	5	5	5
G1 (glass)	5	5	5
G2 (glass)	3	3	3
AG1 (aramid-glass)	3	3	3
B1 (basalt)	3	3	3

Table 4. Tensile tests results: mechanical parameters describing the tensile behavior of the samples.

Sample type		σ_1 [MPa]	σ_2 [MPa]	σ_u [MPa]	ε_1 [%]	ε_2 [%]	ε_u [%]	E_1 [GPa]	E_2 [GPa]	E_3 [GPa]	Failure mode
C1	Average	203	1359	2530	0.051	0.638	1.137	410	197	234	A-B
	CoV [%]	9.9	5.5	5.0	17.0	7.1	4.4	18.6	2.1	3.1	
C2	Average	310	-	1290	0.019	-	0.701	1687	-	190	A-B
	CoV [%]	35.0	-	6.9	20.0	-	10.2	34.9	-	13.9	
G1	Average	125	-	1165	0.055	-	1.542	236	-	70	B
	CoV [%]	6.0	-	3.2	20.2	-	2.4	19.0	-	4.5	
G2	Average	435	-	1096	0.040	-	1.891	1098	-	43	A-B
	CoV [%]	3.9	-	5.3	14.0	-	7.0	12.2	-	8.1	
AG1	Average	363	-	1467	0.009	-	1.218	4203	-	115	A
	CoV [%]	16.3	-	1.6	33.3	-	9.8	19.2	-	8.8	
B1	Average	413	435	1663	0.027	0.430	2.112	1572	5	73	A
	CoV [%]	12.6	10.7	2.7	26.7	5.6	5.5	17.1	19.4	9.6	

Table 5. Results of monotonic and cyclic single-lap shear tests.

Sample type		Failure mode (N° of times)	Average maximum load [kN]	Average peak stress (σ_f) [MPa]	CoV [%]	η [%]	Difference [%]
C1	Monotonic	C(5)	3.838	1438	5.5	56.84	-
	Cyclic	C(5)	4.023	1507	7.8		+ 4.8 %
C2	Monotonic	D(5)	1.182	314	3.9	24.34	-
	Cyclic	D(5)	1.207	321	5.7		+ 2.1 %
G1	Monotonic	E(3) - E*(2)	2.843	790	7.3	67.81	-
	Cyclic	E (4) – E*(1)	3.015	837	7.8		+ 6.1 %
G2	Monotonic	D**(3)	3.033	867	5.3	79.11	-
	Cyclic	D**(3)	3.228	922	2.0		+ 6.4 %
AG1	Monotonic	E(3)	2.963	1275	1.4	86.91	-
	Cyclic	E(3)	3.055	1314	6.2		+ 3.0 %
B1	Monotonic	D(2) – E*(1)	3.635	1141	5.2	68.61	-
	Cyclic	E(2) – E*(1)	3.530	1108	6.5		- 2.9 %

* Partial delamination before fiber tensile failure

** Fiber slippage with final tensile failure of the reinforcement

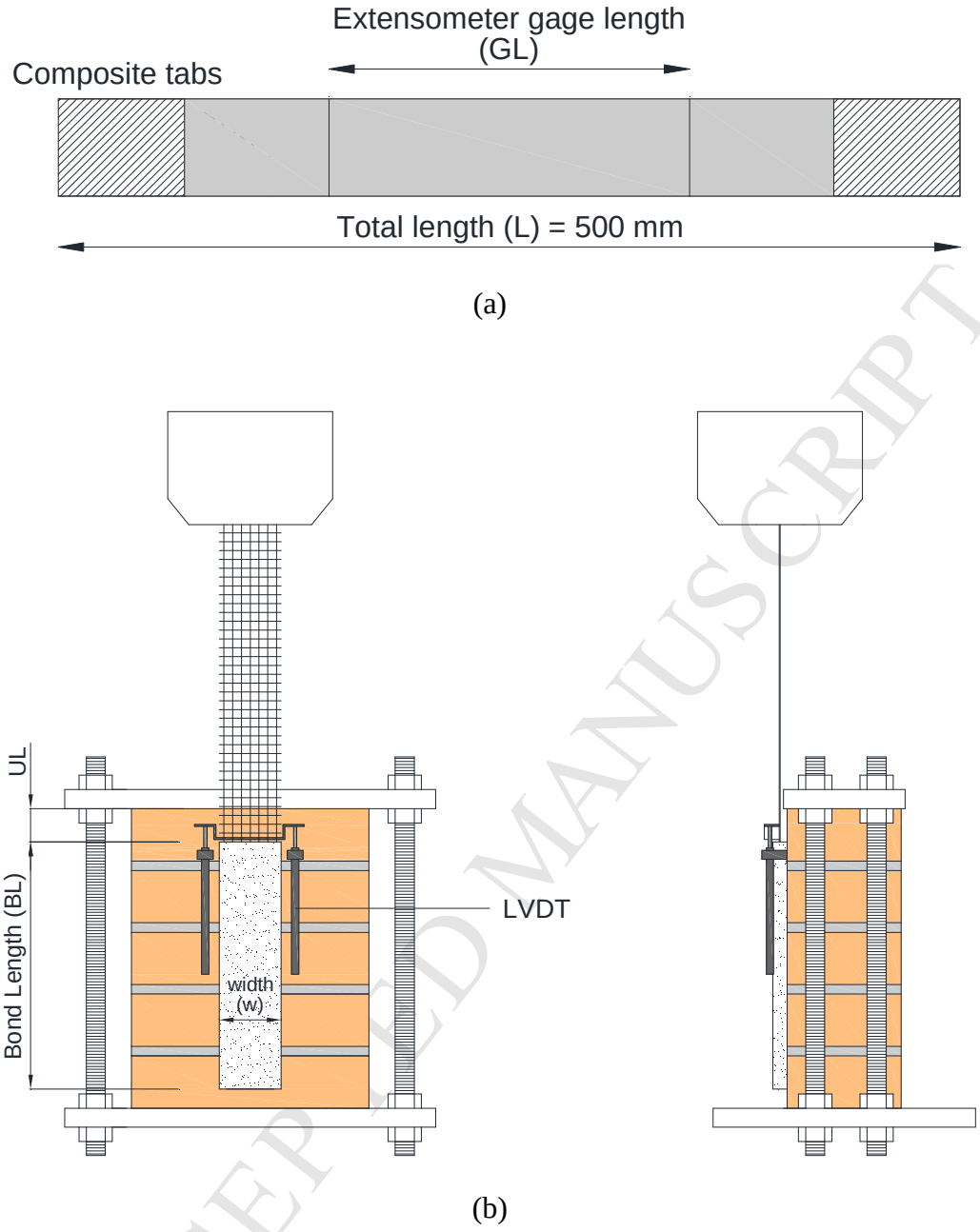

Figure 1. Geometry of the samples: (a) tensile tests; (b) single lap shear tests.

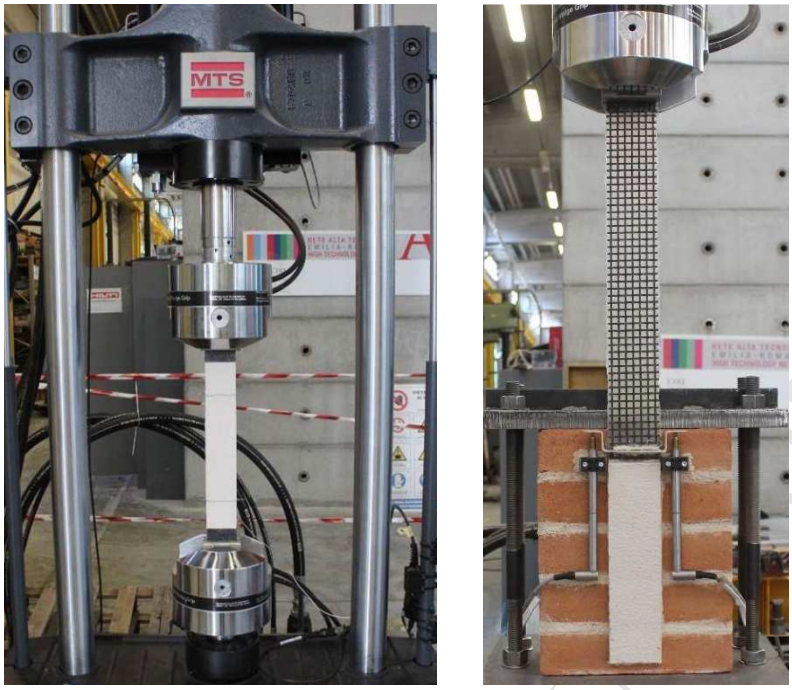

(a) (b)

Figure 2. Experimental set-ups: (a) tensile tests; (b) monotonic and cyclic bond tests.

(a)

(b)

Figure 3. Failure modes identified during tensile tests: (a) Failure mode A (fiber rupture inside the gage length of the extensometer); (b) Failure mode B (tensile failure outside the gage length).

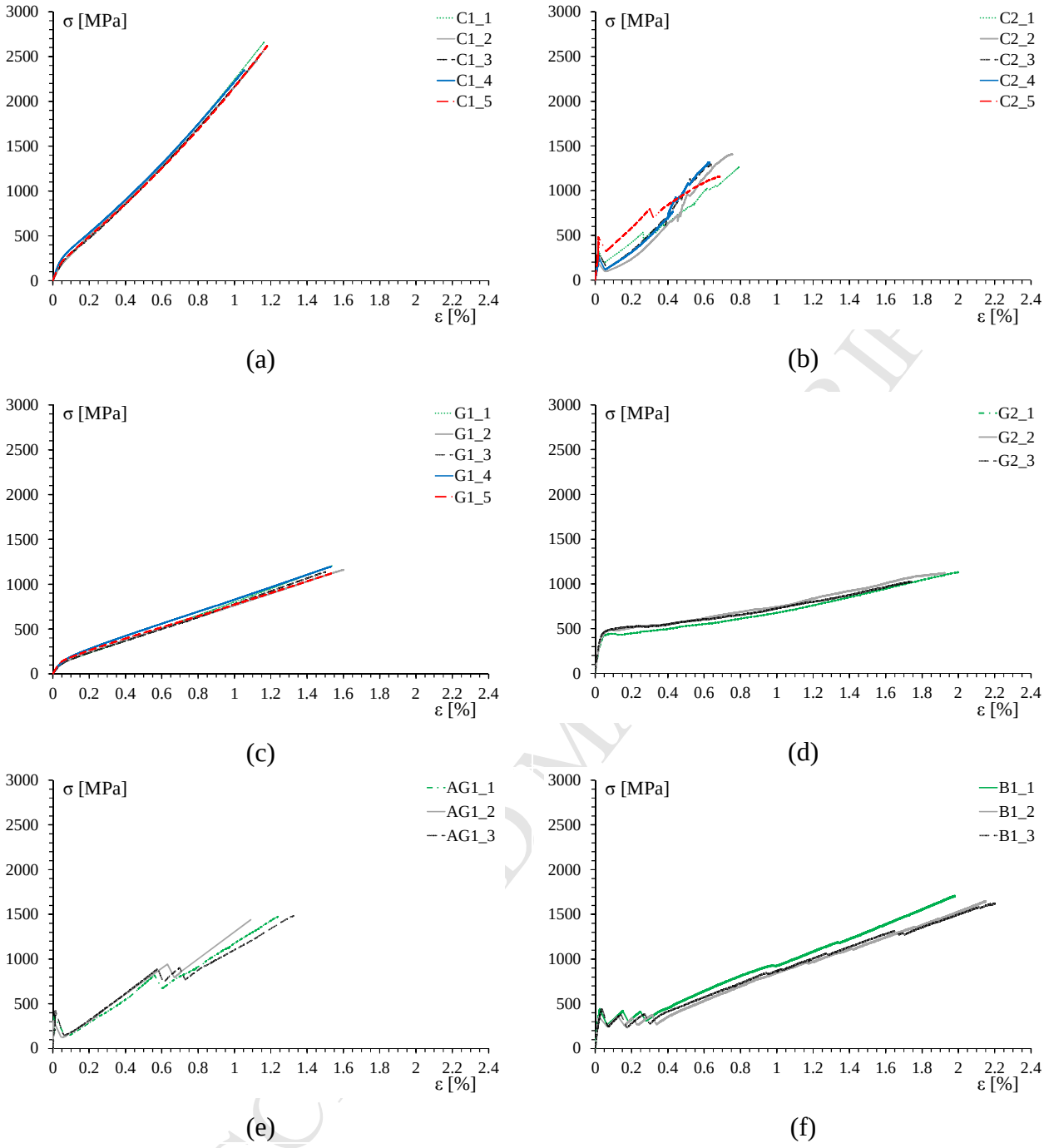

Figure 4. Stress-strain graphs coming from tensile tests on FRCM reinforcements: (a) C1 specimens; (b) C2 samples; (c) G1 specimens; (d) G2 samples; (e) AG1 specimens; (f) B1 samples.

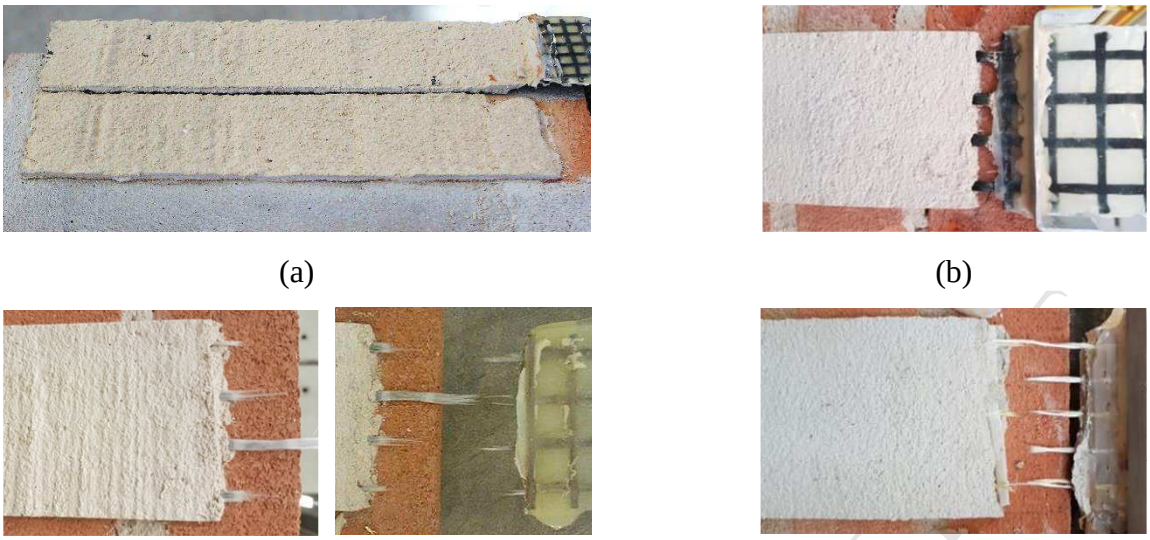

Figure 5. Bond failure modes: (a) Failure mode C (delamination within the inner mortar layer); (b) Failure mode D (fiber slippage within the matrix layers); (c) Failure mode D** (fiber slippage with final tensile failure); (d) Failure mode E (tensile rupture of the fibers outside of the bonded area).

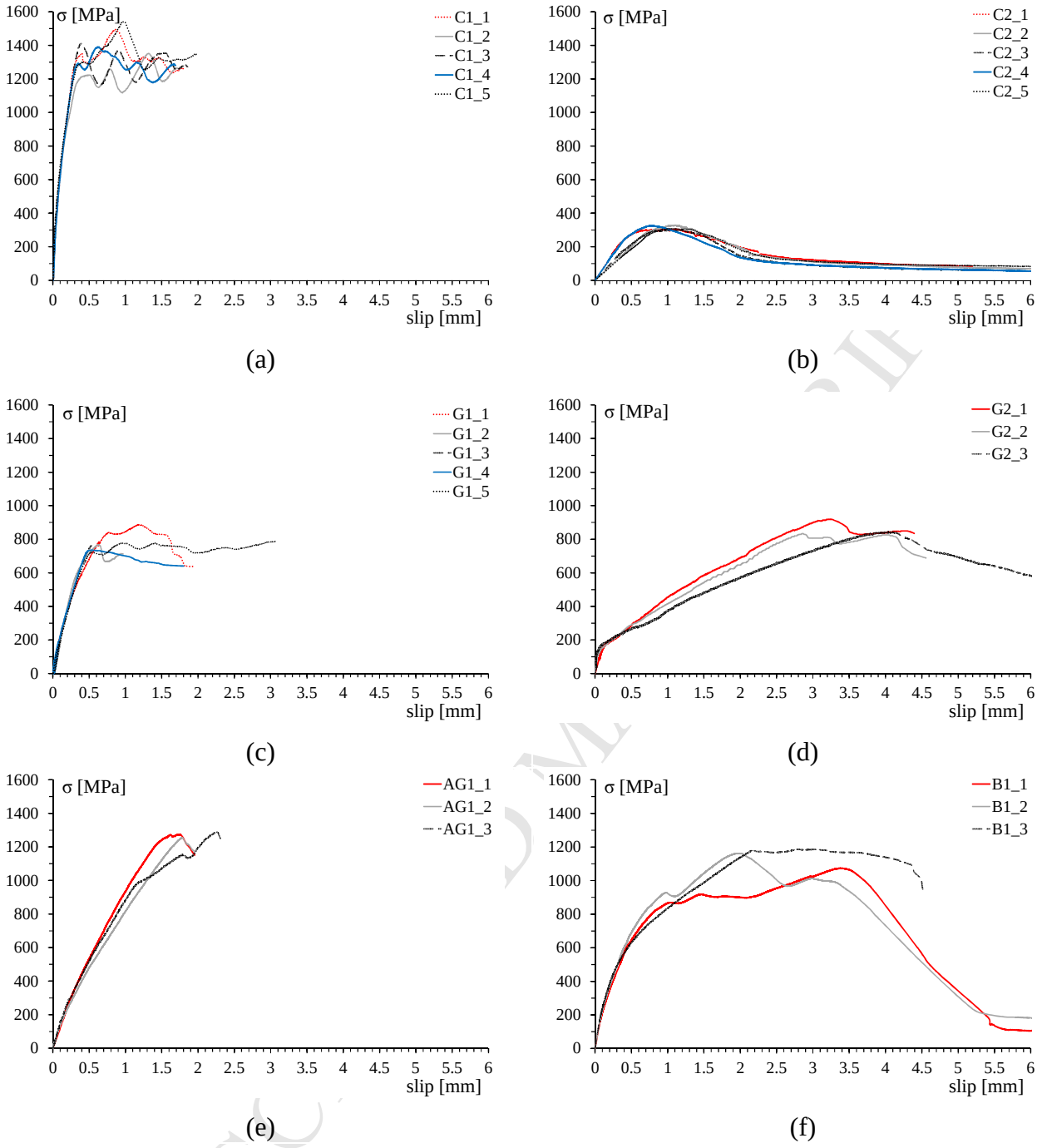

Figure 6. Stress-slip graphs coming from monotonic bond tests on FRCM reinforcements: (a) C1 specimens; (b) C2 samples; (c) G1 specimens; (d) G2 samples; (e) AG1 specimens; (f) B1 samples.

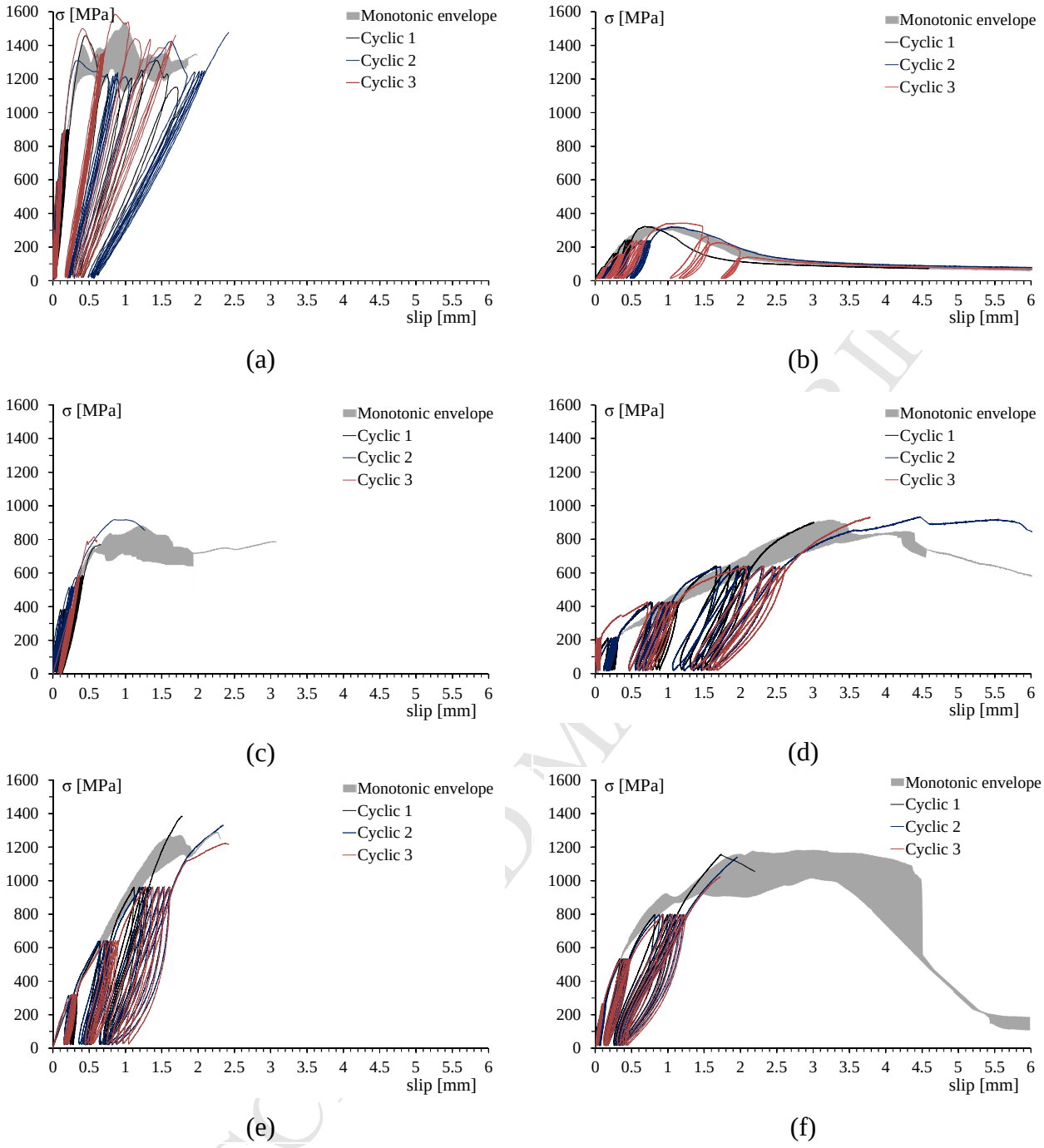

Figure 7. Monotonic and cyclic bond tests comparison: (a) C1 specimens; (b) C2 samples; (c) G1 specimens; (d) G2 samples; (e) AG1 specimens; (f) B1 samples.

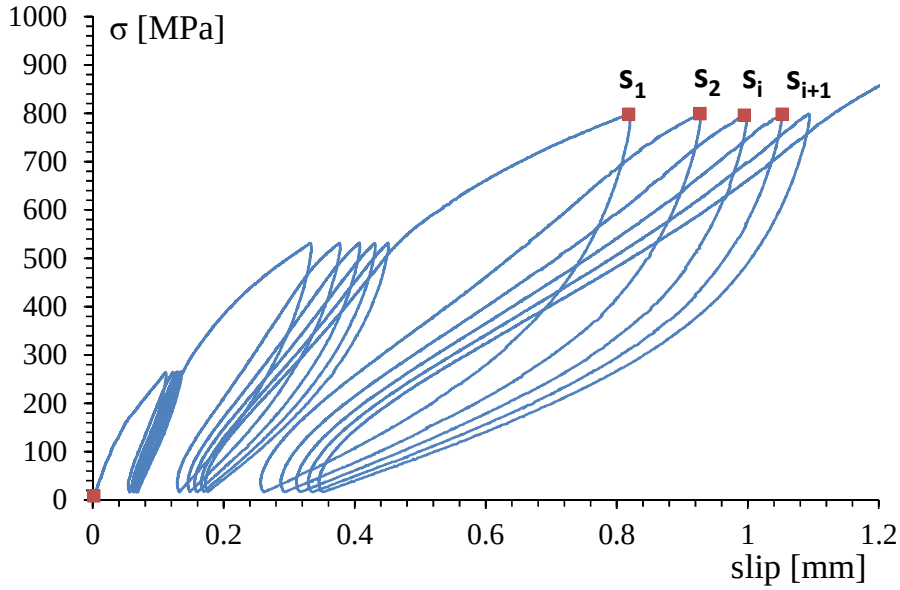

Figure 8. Example of cyclic degradation and Δ parameter calculation.

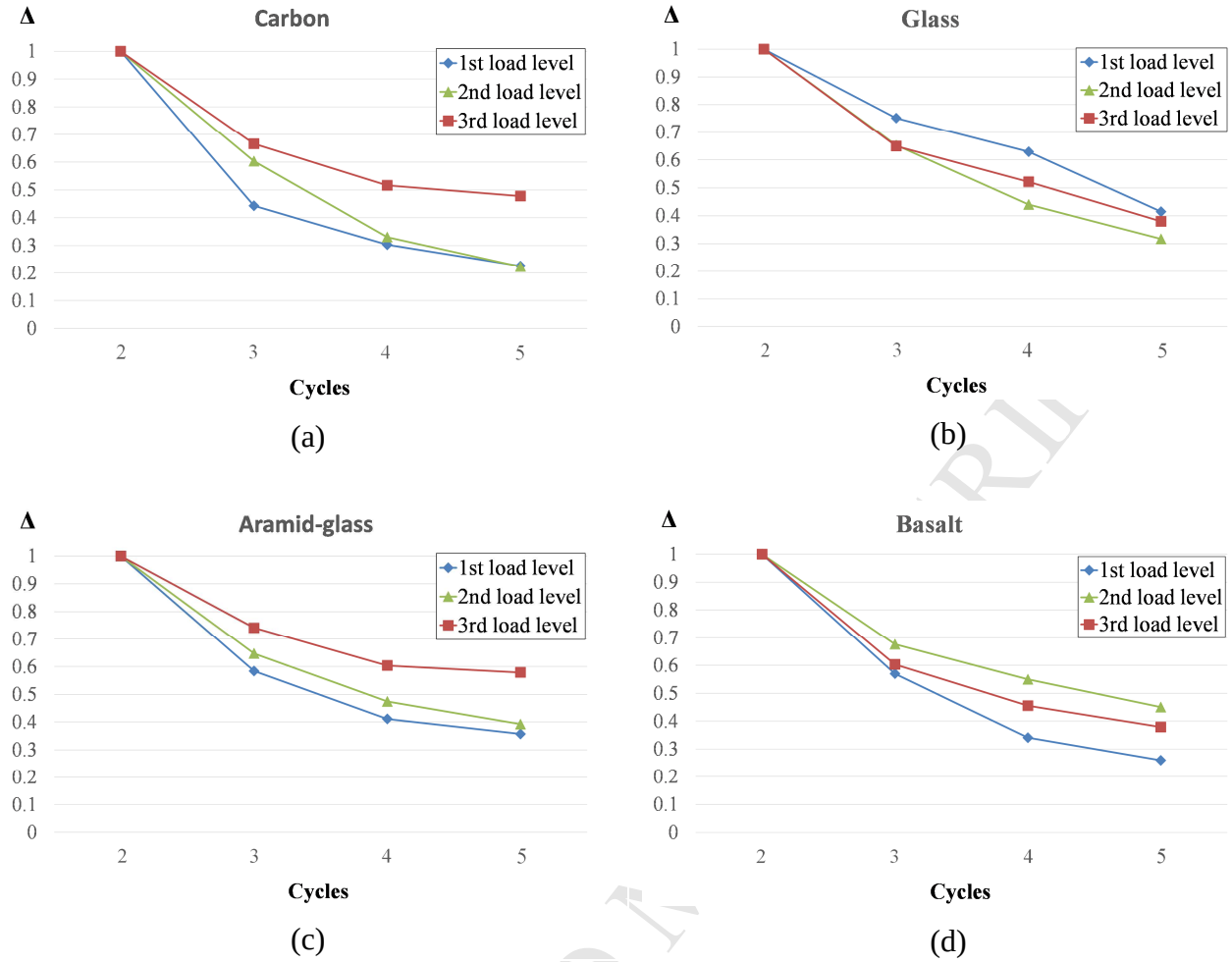

Figure 9. Bond tests - cyclic degradation: (a) carbon samples; (b) glass specimens; (c) aramid-glass samples; (d) basalt specimens.